

Dense Air Quality Maps Using Regressive Facility Location Based Drive By Sensing

Charul Paliwal¹ and Pravesh Biyani¹

¹Indraprastha Institute of Information Technology, Delhi



Abstract—Currently, fixed static sensing is a primary way to monitor environmental data like air quality in cities. However, to obtain a dense spatial coverage, a large number of static monitors are required, thereby making it a costly option. Dense spatiotemporal coverage can be achieved using only a fraction of static sensors by deploying them on the moving vehicles, known as the drive by sensing paradigm. The redundancy present in the air quality data can be exploited by processing the sparsely sampled data to impute the remaining unobserved data points using the matrix completion techniques. However, the accuracy of imputation is dependent on the extent to which the moving sensors capture the inherent structure of the air quality matrix. Therefore, the challenge is to pick those set of paths (using vehicles) that perform representative sampling in space and time. Most works in the current literature for vehicle subset selection focus on maximizing the spatiotemporal coverage by maximizing the number of samples for different locations and time stamps which is not an effective representative sampling strategy and results in noisy imputations. We present regressive facility location based drive by sensing, an efficient vehicle selection framework that incorporates the smoothness in neighboring locations and autoregressive time correlation while selecting the optimal set of vehicles for effective spatiotemporal sampling. We show that the proposed drive by sensing problem is submodular, thereby lending itself to a greedy algorithm but with performance guarantees. We evaluate our framework on selecting a subset from the fleet of public transport in Delhi, India. We illustrate that the method proposed in the paper samples the representative spatiotemporal data against the baseline methods, reducing the extrapolation error on the simulated air quality data. Our method, therefore, has the potential to provide cost effective dense air quality maps.

sampled timestamps. However, the spatial coverage in a region depends on the number of sensors installed which is generally limited owing to the cost constraints. We can leverage the spatial and temporal correlation in the air quality data to perform cost-effective spatiotemporal monitoring. We can share/multiplex an air quality sensor over multiple locations and perform sequential temporal sensing without losing air quality information. Moving sensor paradigm can be a candidate to obtain such dense AQ (Air Quality) map without needing an expensive setup of hundreds of static monitors [2], [3]. With the technological progress in AQ sensing, it is now possible to put these monitors in buses and other public transit and perform spatiotemporal AQ sensing. However, the moving sensors reading would be spatially and temporally sparse and incomplete because of the unavailability of the moving vehicle across all the spatial locations and timestamps.

Thanks to the inherent temporal and spatial redundancy available in the air quality data, one can potentially impute the remaining (incomplete) data by utilising the matrix completion techniques [4], [5] and obtain a dense air quality map in a fraction of the corresponding fixed sensing cost. However, the quality of imputation crucially relies on the “quality” of drive by sensing and the choice of “routes” that vehicles take to sample the air quality.

The problem of dense air quality maps using drive by sensing is defined as: Given a binary bus occupancy data $\mathcal{Y} \in \{0, 1\}^{|\mathcal{L}| \times |\mathcal{T}| \times |\mathcal{B}|}$, where \mathcal{L} denotes the set of locations, \mathcal{T} denotes the set of timestamps and \mathcal{B} denotes the buses. The entry $y_{l,t,b} = 1$ if the bus b samples the location l in the time stamp t . The aim is to pick the best subset of buses $\mathcal{M} \in \mathcal{B}$ that perform representative sampling for the spatiotemporal AQ matrix. Subsequently, by appropriately modeling the spatial and temporal structure present in the AQ data sampled by the set of buses \mathcal{M} , one can extrapolate/impute the missing data in the spatiotemporal matrix. In a nutshell, the aim is to pick those buses that exploit the spatiotemporal structure in the air quality data resulting in an effective imputation and thereby creating dense anytime-anywhere AQ map.

Limited work on selecting the optimal set of vehicles for sensing spatiotemporal data models each entry in the spatiotemporal matrix as independent and tries to maximize the number of entries in the matrix [6]–[8]. Considering all

1 INTRODUCTION

Air pollution has drawn attention in recent years because of its profound effect on people’s health [1]. It is crucial to assess the pollution level in a region by monitoring the air quality levels and recommend strategies to combat pollution. There are significant factors that affect the air quality of an area, such as transportation, electricity, fuel uses, industrial parameters such as power plant emissions, etc. Hence, air quality monitoring is required to make strategies for emission control as well as verifying strategies that control emissions.

The most widely used method to monitor air quality is by using static sensing, that is mounting sensors at fixed locations. The temporal resolution of static sensing is high, i.e., the air quality data is available for almost all the

the locations as independent ignores the correlation across locations, thereby highlighting the sub-optimality of such an approach. Indeed, sampling two consecutive neighborhood locations are less effective than sampling the diverse spread across locations in an area.

Our work exploits the smoothness in the spatial locations to select buses that sample diverse and representative sets of locations. Further, the air quality data for a given location is smooth in time, i.e., the sensor data varies slowly in time with decreasing correlation as the interval increases. Thereby, sampling the consecutive timestamps of a site is a less effective strategy than sampling at distant time stamps. The proposed Regressive Facility Location (RFL) framework encapsulates the temporal smoothness using an autoregressive time series structure to sample the spatiotemporal data. Also, since the future temporal data is not available to create the dense map at a particular timestamp, we use the causal temporal smoothness in the proposed RFL framework. This ensures that if a location l is sampled at a given time, other buses can bypass sampling location l and the nearby locations in the subsequent neighboring future time stamps. The Regressive Facility Location (RFL) framework proposes to encapsulate the slowly varying temporal data pattern into the facility location framework and select the buses such that the sampled locations will be representative of the area and will be diverse across all time stamps.

Practically it is not possible to access the real-world air quality data without deploying the sensors on the selected set of buses. Therefore, to evaluate the performance of the proposed RFL drive by sensing framework, we simulate real-world air quality data. Further, we obtain the dense air quality maps using the matrix completion framework from the sampled spatio-temporal data and observe that RFL provide more accurate dense air quality maps. The overall contribution of our work are:

- 1) We propose Regressive Facility Location (RFL), a novel method to select a fleet of vehicles (buses) for drive by sensing that incorporates the smoothness of the sensor reading across space as well as time to provide effective data sampling.
- 2) We show that the proposed RFL algorithm gain is submodular, therefore a greedy heuristic provides a solution within an approximation ratio of $(1 - \frac{1}{e})$.
- 3) We simulate the smooth data over space and time and sample the area using the proposed drive by sensing framework. To evaluate the performance of the proposed framework, we create dense maps using a matrix completion framework from the sampled data.

1.1 Notations

A tensor is represented by \mathcal{Y} . Matrix is denoted by \mathbf{Y} . A set is denoted by \mathcal{Y} , the number of element in a set is denoted by Y where $Y = |\mathcal{Y}|$, the element of the set is denoted by y .

2 BACKGROUND REVIEW

2.1 Vehicle Subset Selection

There has been limited work on selecting the optimal set of vehicles for sensing spatiotemporal data. Authors in

[8] propose mobile sensor placement for vehicles to maximize coverage. Authors in [6] propose a drive by sensing framework for taxis and buses. Authors in [7] proposed Point of interest oriented (POIs) Bus Selection algorithm to select buses where the coverage of a bus is defined in terms of the POIs. Authors in [9] proposed the optimal placement of reference monitors to make mobile sensors k-hop calibrable. However, the mobile sensors are fixed and reference monitors are optimally selected. All these framework maps the problem of vehicle subset selection to the maximum cover problem or set cover problem to maximize the spatiotemporal coverage.

2.2 Greedy Submodular Maximization

Definition 1: A function f is monotonically non decreasing if $\forall \mathcal{C} \subseteq \mathcal{D}$

$$f(\mathcal{C}) \leq f(\mathcal{D})$$

Definition 2: A function $f: 2^{\mathcal{B}} \rightarrow \mathbf{R}$ is submodular if $\forall \mathcal{C} \subseteq \mathcal{D} \subseteq \mathcal{B}$ and every $b \in \mathcal{B} \setminus \mathcal{D}$

$$f(\mathcal{C} \cup b) - f(\mathcal{C}) \geq f(\mathcal{D} \cup b) - f(\mathcal{D})$$

Given a submodular set function f , maximization of f over all subsets of size at most k of the ground set \mathcal{G} , i.e. $|\mathcal{G}| = k$,

$$f(\mathcal{V}) = \max_{\mathcal{V}: |\mathcal{V}| \leq k} f(\mathcal{V}) \quad (1)$$

is an NP-hard problem [10]. A monotone non decreasing submodular function solution can be approximate by an greedy algorithm within $(1 - \frac{1}{e})$ of the global maximum [11], [12].

2.3 Generating Smooth Graph Signals

To generate a smooth graph signal across nodes, adjacency matrix can be used. Consider a graph with \mathcal{L} set of nodes/locations, the weighted adjacency matrix can be defined as $\mathbf{G} \in \mathbf{R}^{L \times L}$ can be decomposed as.

$$\mathbf{G} = \mathbf{U}\Sigma\mathbf{U}^T$$

The graph Fourier transform of a signal $\mathbf{x} \in \mathbf{R}^L$ is given by $\hat{\mathbf{x}}$.

$$\hat{\mathbf{x}} = \mathbf{U}^{-1}\mathbf{x}$$

The actual signal can be expressed as

$$\mathbf{x} = \mathbf{U}\hat{\mathbf{x}}$$

The signal is smooth in the time domain if the signal is bandlimited in the frequency domain [13]–[17] hence,

$$\hat{\mathbf{x}}_k = 0 \quad \forall k \geq m$$

Therefore

$$\mathbf{x} = \mathbf{U}_{(m)}\hat{\mathbf{x}} \quad (2)$$

where $\mathbf{U}_{(m)} \in \mathbf{R}^{L \times m}$ represents the first m eigenvectors of the matrix \mathbf{G} .

The signal $\hat{\mathbf{x}}$ can be sampled from random normal distribution as described in the literature [14], [16], [17]. Then using the signal $\hat{\mathbf{x}}$ and \mathbf{U} , actual smooth signal can be constructed over the nodes of the graph via Eq. 2. The signal generated will be smooth on the locations only. We simulate real-world air quality data that is smooth in space and time.

2.4 Dense maps using Missing data imputation

Air quality data exhibits both spatial and temporal correlation thereby generating redundancy (not high rank nature) [18], [19]. Low rank matrix completion has been proposed to estimate the missing spatiotemporal data [4], [20]. Further state space model for incorporating the temporal evolution in the matrix completion framework is also proposed in the literature [5], [21], [22]. However, dense air quality maps cannot be computed using the traditional matrix completion framework for the cold start locations. Cold start locations refers to the set of locations that are never sampled by the selected set of buses. Similarity matrix can be exploited to impute the data for the cold start locations [23], [24].

3 BUS SELECTION FRAMEWORK

Bus selection for drive by sensing is defined as follows: We are given a binary bus occupancy tensor $\mathcal{Y} \in \{0, 1\}^{|\mathcal{L}| \times |\mathcal{T}| \times |\mathcal{B}|}$, where \mathcal{L} is the set of locations, \mathcal{T} is the set of timestamps, and \mathcal{B} is the entire set of buses. Buses run on a specific route with a time schedule. The entry $y_{l,t,b} = 1$ denotes the availability of the sensor reading placed at bus b for a particular location l and time slot t . Our work aims to pick k buses from the entire set of buses \mathcal{B} for drive by sensing, where $\mathcal{M} \subset \mathcal{B}$ represents the selected set of buses. For a subset of buses $\mathcal{M} \subset \mathcal{B}$, we define a binary sampling matrix $\Theta \in \{0, 1\}^{L \times T}$ as

$$\Theta(\mathcal{M}) = \max(\sum_{k \in \mathcal{M}} \mathcal{Y}_{l,t,k}, 1) \quad \forall (l \in \mathcal{L}), \quad \forall (t \in \mathcal{T}) \quad (3)$$

The distance between two locations i and j are defined as $\mathbf{D}_{i,j}$. We then define the normalized distance between two locations $\mathbf{ND}_{i,j} = \frac{\mathbf{D}_{i,j}}{\max(\mathbf{D})}$. All the entries in \mathbf{ND} are between 0 and 1. The smaller the normalized distance between two locations, the higher is the similarity. To incorporate the smoothness in the spatial locations, we define the similarity between locations in $\mathbf{S} \in \mathbf{R}^{L \times L}$ as:

$$\mathbf{S}_{i,j} = 1 - \mathbf{ND}_{i,j} \quad (4)$$

3.1 Baseline methods

3.1.1 Max Coverage (MC)

We model our problem as the max coverage problem where each entry in the sampling matrix Θ is considered as an element [8]. We have the set of buses, each bus e samples some elements in the matrix $\Theta(e)$. Max Coverage framework selects the k number of buses, set $\mathcal{M} \subset \mathcal{B}$ where $|\mathcal{M}| = k$ such that entries in the sampling matrix $\Theta(\mathcal{M})$ is maximized. The maximum coverage problem is NP-hard and submodular; there exists a greedy heuristic that provides a solution within an approximation ratio of $(1 - \frac{1}{e})$ [25]. We use Percentage Coverage as a measure for the Max Coverage Algorithm. The gain for Max Coverage to maximize the occupancy of the selected buses \mathcal{M} is defined as

$$PC(\mathcal{M}) = \frac{\sum_{i \in \mathcal{L}, j \in \mathcal{T}} \Theta(\mathcal{M})_{i,j}}{L \times T} * 100 \quad (5)$$

3.1.2 Max Coverage over Location (MCL)

We model our problem as the max coverage over location problem where each location is considered as an element. We have the set of buses, each bus samples some locations over all the timestamps. Max Coverage over location framework selects the k number of buses, set $\mathcal{M} \subset \mathcal{B}$ where $|\mathcal{M}| = k$ such that maximum locations are sampled. In max coverage over location, we are maximizing the number of locations sampled by the selected buses, while in max Coverage framework, we are maximizing the entries of the sampling matrix Θ to increase the coverage over location as well as time. We use Percentage Stop coverage as a measure for the Max Coverage over Location algorithm as shown in Eq. 6.

$$PSC(\mathcal{M}) = \frac{\sum_{i \in \mathcal{L}} \max\{\sum_{k \in \mathcal{M}, j \in \mathcal{T}} \mathcal{Y}_{i,j,k}, 1\}}{L} * 100 \quad (6)$$

3.2 Facility Location over space (FLS)

Max coverage and max coverage location treat every location as independent while selecting the set of buses, which sample the spatiotemporal matrix. However, a correlation exists across the locations readings; the sensor readings will be smooth over neighboring locations. We thereby use Facility Location over space (FLS) to model the smoothness in the locations using a similarity matrix.

For the selected set of buses \mathcal{M} , the sampling matrix is defined in Eq.3. For a time stamp t , the sampled locations by the set of buses \mathcal{M} is defined as $\theta_t(\mathcal{M})$,

$$\theta_t(\mathcal{M}) = \{i\} \quad \forall \Theta_{i,t}(\mathcal{M}) = 1$$

$$FLS(\mathcal{M}) = \frac{\sum_{t \in \mathcal{T}} \sum_{l \in \mathcal{L}} \pi_t^l(\mathcal{M})}{L \times T} \quad (7)$$

$$\pi_t^l(\mathcal{M}) = \max_{\forall m \in \theta_t(\mathcal{M})} (\mathbf{S}_{l,m}) \quad (8)$$

We compute the maximum pairwise similarity between all the locations ($i \in \mathcal{L}$) and the sampled set locations denoted by $\theta_t(\mathcal{M})$ for a timestamp t . The gain defined in Eq. 7 is maximized when the pairwise similarities between the locations and the nearest chosen location in the selected set of buses are maximized for all the timestamps. This ensures that we pick the buses that sample the locations that are representative of the entire area for all the timestamps.

Theorem 1: The Function defined in Eq. 7 is monotone submodular. Therefore a greedy heuristic provides a solution within an approximation ratio of $(1 - \frac{1}{e})$.
Proof: The proof is carried out in the appendix.

3.3 Regressive Facility Location (RFL)

FLS selects the buses that sample representative locations across all timestamps. However, fails to capture the temporal correlation while selecting the set of buses and treat all timestamps as independent. The sensor observations of a location over time are not independent and varies slowly over time. The FLS framework can be modified to incorporate the space and time similarity as shown in Fig. 1.

The modified framework incorporates the temporal causal similarity i.e., the future time data is not available to

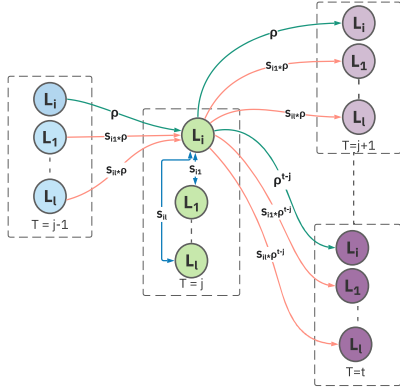


Fig. 1: Spatial and temporal similarity

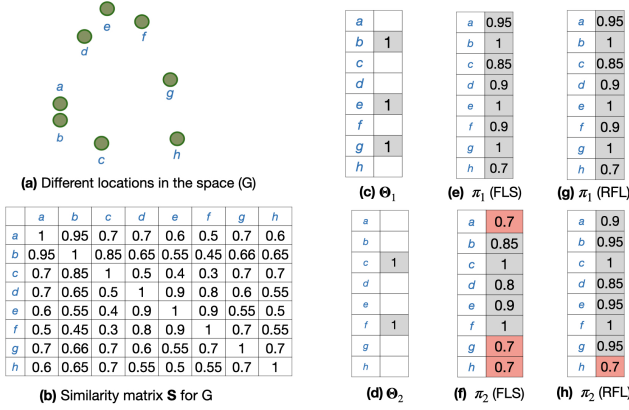


Fig. 2: (a) Represents the locations of an example graph G, (b) The Similarity matrix S for Graph G, (c)-(d) Sampling matrix Θ for time $t=1$ and 2, (e)-(f) π_t for FLS, (g)-(h) π_t for RFL.

infer the previous time stamps using ρ . The Facility location incorporating the space and time causal similarity is called Facility Location over Space-Time (FLST). The similarity coefficients for location i and timestamp j is denoted in Fig. 1. Blue edges in the graph denote the similarity between different locations for a particular timestamp j . Note that $\rho = 0$ is a special case for FLS, and only blue edges are used for similarity in the FLS framework. FLST models the inter-temporal similarity for a particular location using ρ and is denoted by green edges in Fig 1. The inter location and inter-temporal similarity are denoted by orange edges. Directed edges represent the similarity from one node to the other. Note that since we are modeling the temporal causal similarity, reading at location i is relevant only for the locations at future timestamps. The gain for the FLST is defined as

$$FLST(\mathcal{M}) = \frac{\sum_{t \in \mathcal{T}} \sum_{l \in \mathcal{L}} \pi_t^l(\mathcal{M})}{L \times T} \quad (9)$$

$$\pi_t^l(\mathcal{M}) = \max_{j, m \in \Theta(\mathcal{M})} (\mathbf{S}_{l,m} * \mathbf{T}_{t,j}) \quad (10)$$

where the Temporal causal similarity is defined as

$$\mathbf{T}_{t,j} = \begin{cases} \rho^{t-j}, & t \geq j \\ 0, & t < j \end{cases} \quad (11)$$

It is computationally expensive to compute the Eq. 9 since the comparison for every location and time is done for all

the sampled data Θ . Therefore, we propose a fast algorithm that optimizes the gain defined in Eq. 9, with a reduced computational complexity.

Let θ_t be the set of locations that corresponds to sampled locations in the sampling matrix Θ for time stamp t . For $\pi_0 = 0$, $\rho \in [0, 1]$, the regressive facility location gain is defined by

$$RFL(\mathcal{M}) = \frac{\sum_{t \in \mathcal{T}} \sum_{l \in \mathcal{L}} \pi_t^l(\mathcal{M})}{L \times T} \quad (12)$$

$$\pi_t^l(\mathcal{M}) = \max((\mathbf{S}_{l,m})_{\forall m \in \theta_t(\mathcal{M})}, \rho \pi_{t-1}^l(\mathcal{M})) \quad \forall l \in \mathcal{L} \quad (13)$$

Corollary 1: FLST gain defined via Eq. 28 is equivalent to the RFL gain defined via Eq. 41.

Proof: The proof is carried out in the appendix.

RFL encapsulates the temporal correlation to calculate the gain for π_t^l by using π_{t-1}^l . The idea for incorporating the temporal sampling diversity is if the location is sampled at time t_1 , then the subsequent neighboring time sampling would not be the best informative sampling as the data is smooth over time. In RFL, we incorporated the smoothness over time as shown in Fig. 2. Given that a location g is sampled at time $t = 1$, then the π_2 gain in the next timestamp is lower in FLS than RFL. Moreover, suppose we have two adjacent locations a and b , that are neighboring nodes with high similarity. In that case, sampling the location b at timestamp t_1 will also provide information for the location a at subsequent neighboring time stamps as shown in Fig. 2. The greedy approach for the Facility location over space is shown in Algorithm 1.

Theorem 2: The Function defined in Eq. 40 is monotone submodular. Therefore a greedy heuristic provides a solution within an approximation ratio of $(1 - \frac{1}{e})$.

Proof: The proof is carried out in the appendix.

Computational Complexity: For each $l \in \mathcal{L}$ and $t \in \mathcal{T}$ computing $\pi_t^l(\mathcal{M})$ via Eq. 8 requires Λ comparisons where $\Lambda < L$ hence the computational complexity for each iteration of the greedy algorithm for all the buses in FLS is $O(\Lambda L T B)$. For each $l \in \mathcal{L}$ and $t \in \mathcal{T}$ computing $\pi_t^l(\mathcal{M})$ via Eq. 28 requires ΛT comparisons, hence a cost of $O(\Lambda L T^2 B)$ for FLST. We reduce the computation complexity of RFL by computing $\pi_t^l(\mathcal{M})$ via Eq. 41 to $O(\Lambda L T B)$.

Algorithm 1 Regressive Facility Location

Input: $k, \mathcal{B}, \mathcal{Y}, \rho, \mathbf{S}$

Output: $\mathcal{M} \subset \mathcal{B}$ of size k

Initialization: $\mathcal{M} \leftarrow \emptyset; \pi_0 = 0$

- 1: **for** $i=1$ to k **do**
- 2: **for** each $e \in \mathcal{B}$ **do**
- 3: $\Theta(\mathcal{M} \cup e) = \max(\sum_{k \in \mathcal{M} \cup e} \mathcal{Y}_{i,j,k}, 1)$
- 4: **for** each $t \in \mathcal{T}$ **do**
- 5: $\theta_t(\mathcal{M} \cup e) = \{i\} \quad \forall \Theta_{i,t}(\mathcal{M} \cup e)|_{=1}$
- 6: Compute $\pi_t^l(\mathcal{M} \cup e)$ using Eq. 41 ($\forall l \in \mathcal{L}$)
- 7: **end for**
- 8: $f(\mathcal{M} \cup e) = \frac{1}{L \times T} \sum_{t=1}^T \sum_{l=1}^L \pi_t^l(\mathcal{M} \cup e)$
- 9: **end for**
- 10: $e^* = \arg \max_e f(\mathcal{M} \cup e)$
- 11: $\mathcal{M} \leftarrow \mathcal{M} \cup \{e^*\}$
- 12: **end for**

4 EXPERIMENTATION

4.1 Simulating Real World AQ data

4.1.1 Similarity matrix

To simulate the real world AQ data on the set of location \mathcal{L} and timestamps \mathcal{T} , we learn the similarity matrix based on the static real world of Delhi [26]. It contains the AQ data for 33 locations for 3 months. We define the entry of the Similarity matrix $\mathbf{G}_{i,j} = \exp(-\lambda d_{i,j})$ where $d_{i,j}$ is the distance between the two locations i and j . We learn the parameter λ using linear regression and it is observed to be 0.07676 for the AQ data [26]. We then compute the similarity matrix \mathbf{G} for the set of location \mathcal{L} based on the actual distance between locations $d_{i,j}$. We learn the temporal similarity matrix from the data [26] and use it as a temporal similarity matrix \mathbf{H} .

To generate a spatiotemporal matrix \mathbf{Y} that varies smoothly over space and time, we use two variants described in the following sections.

4.1.2 Simulated Data 1

- We first factorize the actual matrix $\mathbf{Z} \in \mathbf{R}^{L \times T}$ as

$$\mathbf{Z} = \mathbf{A}\mathbf{B}^T$$

where $\mathbf{A} \in \mathbf{R}^{L \times r}$ and $\mathbf{B} \in \mathbf{R}^{T \times r}$.

- We construct the matrix \mathbf{A} for the locations using the \mathbf{G} and a bandlimited signal. The similarity matrix \mathbf{G} can be decomposed as

$$\mathbf{G} = \mathbf{U}\Sigma\mathbf{U}^T$$

We generate the matrix \mathbf{A} with rank r as defined in Eq. 2 as.

$$\mathbf{a}_i = \mathbf{U}_{(m)}\hat{\mathbf{a}}_i \quad (\forall i = 1 \text{ to } r)$$

where a_i represents the i^{th} column of matrix \mathbf{A} , a_i is sampled from a random normal distribution with standard deviation (0.5).

- Similarly we construct the matrix \mathbf{B} for time stamps using \mathbf{H} and a bandlimited signal.

$$\mathbf{H} = \mathbf{V}\Lambda\mathbf{V}^T$$

$$\mathbf{b}_i = \mathbf{V}_{(n)}\hat{\mathbf{b}}_i \quad (\forall i = 1 \text{ to } r)$$

- The overall data \mathbf{Y} is generated using \mathbf{A} , \mathbf{B} and noise signal n distributed as zero mean and std of 0.001.

$$\mathbf{Y} = \mathbf{A}\mathbf{B}^T + \mathbf{N}$$

We run the experiments for randomly generated 30 spatiotemporal matrix \mathbf{Y} , where m is randomly chosen from 5 to 15, n is chosen from 5 to 15, r is chosen randomly from 20 to 30.

4.1.3 Simulated Data 2

To generate a smooth signal over space and time we used the framework described in paper [27].

$$\mathbf{a}_t = \mathbf{U}_{(m)}\hat{\mathbf{a}}_t \quad (14)$$

The observed signal can be generated by the following Eqs:

$$\mathbf{y}_t = \mathbf{z}_t + \mathbf{n}_t \quad (15)$$

$$\mathbf{z}_t = \mathbf{R}\mathbf{z}_{t-1} + \mathbf{a}_t \quad (16)$$

The state transition matrix \mathbf{R} is defined as a general diagonal matrix $\mathbf{R} = \text{diag}(c_1, c_2, \dots, c_T)$, where each c represents the autocorrelation coefficient that describes the time correlation of the data with the delayed (one time lag) data. We randomly generate 30 spatiotemporal matrix with c as 1, m is randomly chosen from 5 to 15 and r is chosen randomly from 20 to 30.

4.2 Creating Dense Maps from Sampled Data

Dense AQ map can be created by first selecting the \mathcal{M} set of buses then sampling the data $\hat{\mathbf{Y}}$ from the simulated ground truth AQ matrix \mathbf{Y} based on the sampling matrix $\Theta(\mathcal{M})$. The final step is to impute the missing data in the matrix $\hat{\mathbf{Y}}$. To evaluate the performance, we compute the MRE score for the missing data imputation. There exist a problem of cold start while imputation, i.e., some of the locations are not sampled at all by the selected set of buses. Therefore, we use an extended version of the matrix imputation method that handles cold start cases. The matrix completion framework (VBMC) proposed in paper [20] imposes a low rank structure on the data to impute the missing data as:

$$\mathcal{L}_1 = \min_{\mathbf{A}, \mathbf{B}} \|\mathbf{P}_\Omega(\mathbf{Y} - \mathbf{A}\mathbf{B}^T)\|_F \quad (17)$$

where $\mathbf{A} \in \mathbf{R}^{L \times r}$ and $\mathbf{B} \in \mathbf{R}^{T \times r}$ and $r = \text{rank}(\mathbf{Y}) \ll \min(L, T)$ Further, VBSF [5] add a regularization on the matrix \mathbf{B} to incorporate the temporal evolution in addition to the low rankness (Eq. 52) as

$$\mathcal{R}(\mathbf{B}) = \sum_{i=1}^T \|\mathbf{b}_i - \mathbf{F}\mathbf{b}_{i-1}\| \quad (18)$$

However, these framework does not incorporate for the cold start locations. Incorporating the similarity matrix \mathbf{G} along with the low rank matrix completion framework can tackle the cold start problem [23], [24].

$$\mathcal{L}_2 = \min_{\mathbf{A}, \mathbf{C}} \|\mathbf{G} - \mathbf{A}\mathbf{C}^T\|_F \quad (19)$$

We use Variational Bayesian Matrix Completion (Cold start) and Variational Bayesian Subspace Filtering (Cold start) as the extended matrix completion frameworks that handles the cold start location data imputation to evaluate the performance of the dense AQ maps. We impute the missing data using VBMC(CS) where we optimize the Eqs. (52, 54). We also impute the missing data using VBSF(CS) where we optimize the Eqs. (52, 53, 54).

4.3 Dataset

We use the Delhi Bus GTFS data [28] to obtain the bus occupancy tensor defined by $\mathcal{Y} \in \{0, 1\}^{L \times T \times B}$

- **Locations (L):** There are total 3210 bus stops. We sample L stops such that the minimum distance between the stops should be d . The total number of locations L is 824 when $d = 500$ m.
- **Time stamps (T):** We use 10 min sampling from 6 am to 10 pm, resulting in $T=96$ as the buses run during this time.
- **Buses (B):** The number of buses B is 1476.

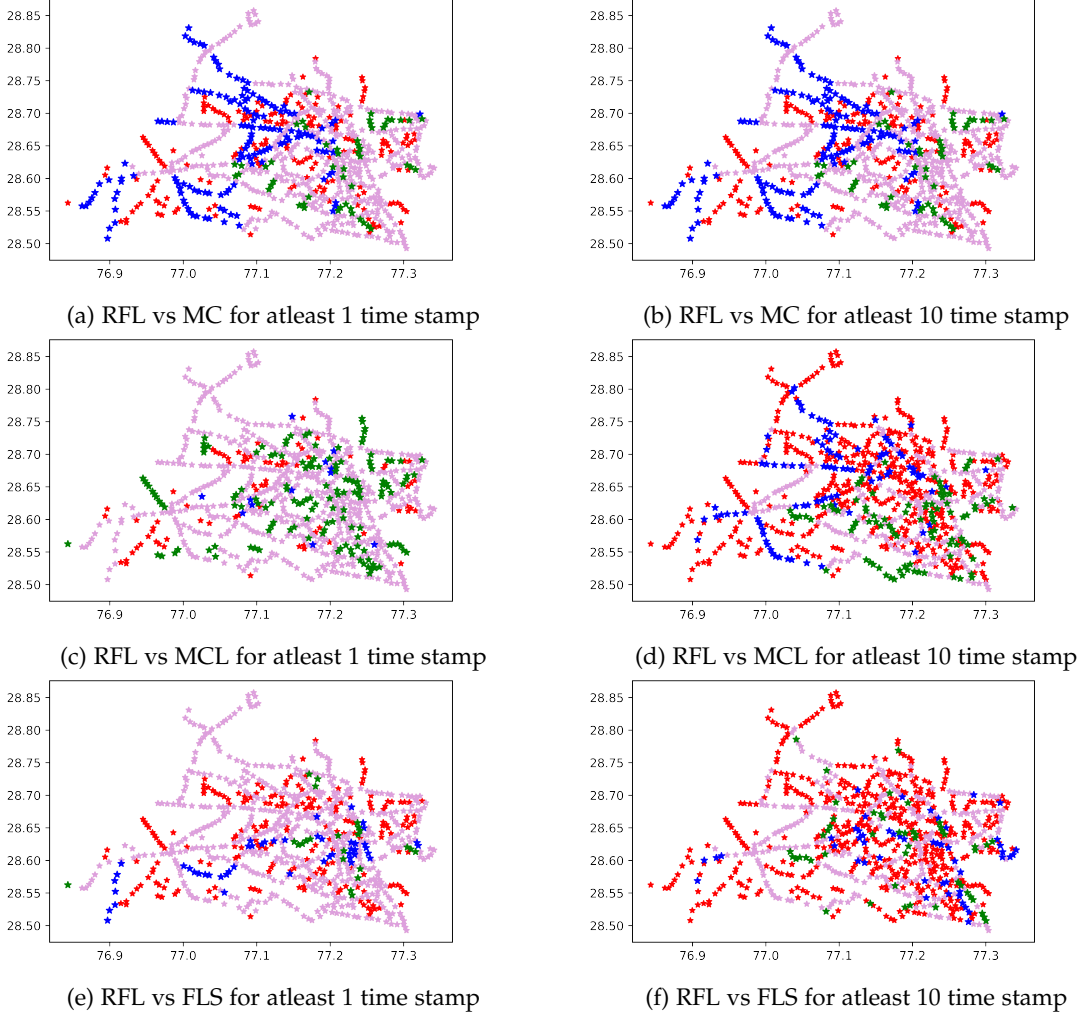


Fig. 3: Coverage plots for all the locations of Delhi for selected bus $k=30$. Red points denote the point not sampled by both RFL and comparison Framework, Pink points denote the points sampled by both RFL and comparison Framework, Blue points denote the points sampled by RFL but not the comparison framework, Green points denote the points sampled by comparison framework but not the RFL

	$k = 20$				$k = 35$				$k = 50$			
	PSC	PC	FLS	RFL	PSC	PC	FLS	RFL	PSC	PC	FLS	RFL
Random bus	56.796	4.612	90.202	91.936	59.102	6.593	90.379	91.563	64.078	10.584	92.515	93.579
Max Coverage	55.218	7.357	91.867	93.163	68.932	11.983	93.801	94.693	79.49	16.117	95.089	95.764
Max Cov Loc	80.704	5.141	90.719	92.593	92.233	7.756	92.734	94.143	96.359	10.293	93.935	94.941
FLS	60.316	6.279	93.164	94.159	73.908	10.685	94.924	95.673	75.728	14.482	95.804	96.363
RFL($\rho = 0.95$)	58.981	6.349	93.122	94.201	71.845	10.628	94.885	95.654	75.85	14.629	95.785	96.392
RFL($\rho = 0.98$)	60.68	6.504	93.16	94.324	72.816	10.761	94.875	95.724	79.369	14.759	95.754	96.414
RFL($\rho = 0.99$)	64.442	6.394	92.842	94.223	73.908	10.68	94.812	95.691	79.126	14.525	95.665	96.385
RFL($\rho = 1$)	71.845	4.949	91.019	92.795	86.529	8.628	93.375	94.614	93.204	12.141	94.472	95.443

TABLE 1: Performance Comparison for selecting k buses

k	Simulated Data 1							Simulated Data 2						
	Random	MC	MCL	FLS	RFL95	RFL98	RFL1	Random	MC	MCL	FLS	RFL95	RFL98	RFL1
20	70.595	39.333	55.582	31.71	31.395	28.507	55.577	70.239	40.13	40.225	27.68	28.03	25.85	43.70
35	47.062	22.29	27.938	10.69	11.065	10.664	21.209	40.26	19.906	16.293	8.395	9.433	8.563	13.75
50	31.6	14.193	16.62	7.465	7.367	6.983	13.997	26.674	11.699	10.822	5.228	5.62	4.251	8.126
75	23.546	11.275	11.296	5.312	5.07	5.065	10.832	19.46	8.448	7.197	2.736	2.627	2.532	7.263
100	18.844	10.375	8.65	4.289	4.271	4.112	7.517	14.732	8.035	5.785	1.973	1.817	1.79	4.487

TABLE 2: MRE for Dense Map using VBMC(CS)

k	Simulated Data 1							Simulated Data 2						
	Random	MC	MCL	FLS	RFL95	RFL98	RFL1	Random	MC	MCL	FLS	RFL95	RFL98	RFL1
20	90.788	37.538	73.922	36.585	36.749	33.602	76.477	77.619	35.275	53.419	30.424	31.479	28.864	57.799
35	44.446	21.008	26.995	10.934	11.609	10.124	19.386	39.429	20.8	19.972	9.817	11.193	9.297	14.858
50	27.766	13.303	15.125	7.018	7.492	6.574	11.678	28.65	13.526	11.627	5.801	6.398	4.904	8.027
75	20.34	10.068	10.15	4.528	4.586	4.52	8.842	21.873	9.704	7.38	2.581	2.591	2.581	5.178
100	16.33	9.52	7.187	3.809	3.769	3.684	6.385	16.922	9.201	5.243	1.76	1.638	1.524	3.547

TABLE 3: MRE for Dense Map using VBSF(CS)

The entries in $y_{l,t,b} = 1$ if bus b is in the 500 meter radius of location l for the time stamp t .

4.4 Evaluation Metrics

The evaluation metrics used for the performance comparison are defined as

- Percentage Stop coverage(PSC) is defined in Eq. (6).
- Percentage Coverage (PC) is defined in Eq. (5)
- FLS gain defined in Eq. 7
- RFL gain defined in Eq. 40 for $\rho = 0.98$
- Mean Relative Error (MRE): $\frac{\|\mathbf{Y} - \hat{\mathbf{Y}}\|}{\|\mathbf{Y}\|}$, where $\hat{\mathbf{Y}}$ is the estimate of \mathbf{Y} .

Mean Relative Error is used to evaluate the performance of imputed dense AQ maps.

4.5 Performance Comparison

4.5.1 Effect of ρ in RFL:

As the ρ increases, PSC increases. For $\rho = 1$, the performance is comparable to the MCL, since if a location is sampled for a timestamp, the gain corresponding to sampling other timestamps will be zero; therefore MCL will select the buses that sample different locations to increase the Percentage stop coverage (PSC). However, the performance of RFL ($\rho = 1$) worsens for PC, FLS and RFL. For $\rho = 0.95$, the performance is comparable to the FLS as the effect of temporal correlation decreases with time in RFL for lower values of ρ . Since the FLS does not incorporate the temporal correlation in the framework and can sample the same set of representative locations across timestamps, we observe a reduced PSC for RFL ($\rho = 0.95$) and FLS. We observe similar performance for RFL($\rho = 0.98$) and RFL($\rho = 0.99$). However we observe an improved FLS score for RFL($\rho = 0.98$) through out as compared to RFL($\rho = 0.99$). Therefore we evaluate the performance of RFL for $\rho = 0.98$ rather than $\rho = 0.99$ for dense map creation.

4.5.2 Coverage Plot:

To demonstrate the representations in space and time, we plot the coverage plot as shown in Fig 3. Every point on the plot is one of the bus stop locations. Fig 3 (a-c) denotes the locations that are sampled for atleast one timestamp, thereby illustrating the overall stops coverage. Fig 3 (d-f) represents the locations that are sampled for atleast 10 timestamps, thereby demonstrating the temporal coverage for the sampled stops. Pink points denote the locations sampled by both the RFL and the compared framework. Blue points denote the point sampled by the RFL but not the compared framework, green points denote the points

sampled by the comparison framework but not the RFL and red points denote the points not sampled by RFL and the compared framework. From Fig. 3(a,d), it is observed that the MC does not sample a diverse set of locations. MCL provides improved spatial coverage, however the temporal coverage is worse as compared to RFL as shown in Fig. 3(b,e). It can also be observed that RFL samples a diverse set of locations than FLS as shown in Fig 3(c,f).

4.5.3 Dense AQ map MRE:

The MRE scores for creating dense AQ map is shown in Table 2, 3. For simplicity we denote the RFL($\rho = 0.95$) as RFL95. It is observed that RFL($\rho = 0.98$) outperforms all the baseline algorithms for dense map creation VBMC(CS) and VBSF(CS). Since the generated data have temporal correlation thereby VBSF(CS) performance is better than VBMC(CS) for most of the cases, especially for higher bus sampling. However, for the lower sampling of buses (20), it is observed that VBMC(CS) performs better as there are significantly lower samples to learn the temporal pattern along with the low rankness.

All the experiments are run on Matlab/Python with the system configuration of 2.3 GHz and 16 GB RAM.

5 CONCLUSION

The anytime-anywhere AQ map is the holy grail of AQ monitoring and is crucial for combating air pollution, especially in the developing world. To obtain a dense air quality map, the cities may require only a small fraction of moving sensors as compared to all static sensors setup. The spatiotemporal correlation in the air quality data can be leveraged to select the moving sensor for sampling and to facilitate an effective spatiotemporal extrapolation on the sampled data. This paper proposes a Regressive Facility Location for drive-by sensing to select the set of buses that samples the spatiotemporal AQ data. It is shown that the chosen set of buses provides representative coverage across space and time. We further obtain the dense AQ maps using the matrix completion framework from the sampled spatiotemporal data and observe that RFL provides more accurate dense AQ maps.

6 ACKNOWLEDGEMENT

The authors would like to thank Dr. Rishabh Iyer (University of Texas, Dallas) for his suggestions.

REFERENCES

- [1] P. Florina and H. W. Ven-dee, "The global distribution of air pollution," <https://datatopics.worldbank.org/world-development-indicators/stories/the-global-distribution-of-air-pollution.html>, 2019.

- [2] A. Anjomshoa, F. Duarte, D. Rennings, T. J. Matarazzo, P. deSouza, and C. Ratti, "City scanner: Building and scheduling a mobile sensing platform for smart city services," *IEEE Internet of things Journal*, vol. 5, no. 6, pp. 4567–4579, 2018.
- [3] D. Hasenfratz, O. Saukh, C. Walser, C. Hueglin, M. Fierz, T. Arn, J. Beutel, and L. Thiele, "Deriving high-resolution urban air pollution maps using mobile sensor nodes," *Pervasive and Mobile Computing*, vol. 16, pp. 268–285, 2015.
- [4] M. T. Asif, N. Mitrovic, J. Dauwels, and P. Jaillet, "Matrix and tensor based methods for missing data estimation in large traffic networks," *IEEE Trans. Intell. Transp. Syst.*, vol. 17, no. 7, pp. 1816–1825, 2016.
- [5] C. Paliwal, U. Bhatt, P. Biyani, and K. Rajawat, "Traffic estimation and prediction via online variational bayesian subspace filtering," *IEEE Transactions on Intelligent Transportation Systems*, 2021.
- [6] D. Agarwal, S. Iyengar, M. Swaminathan, E. Sharma, A. Raj, and A. Hatwar, "Modulo: Drive-by sensing at city-scale on the cheap," in *Proceedings of the 3rd ACM SIGCAS Conference on Computing and Sustainable Societies*, 2020, pp. 187–197.
- [7] Y. Gao, W. Dong, K. Guo, X. Liu, Y. Chen, X. Liu, J. Bu, and C. Chen, "Mosaic: A low-cost mobile sensing system for urban air quality monitoring," in *IEEE INFOCOM 2016-The 35th Annual IEEE International Conference on Computer Communications*. IEEE, 2016, pp. 1–9.
- [8] J. Ali and V. Dyo, "Coverage and mobile sensor placement for vehicles on predetermined routes: A greedy heuristic approach," 2017.
- [9] K. Fu, W. Ren, and W. Dong, "Multihop calibration for mobile sensing: K-hop calibratability and reference sensor deployment," in *IEEE INFOCOM 2017-IEEE Conference on Computer Communications*. IEEE, 2017, pp. 1–9.
- [10] S. Fujishige, *Submodular functions and optimization*. Elsevier, 2005.
- [11] G. Calinescu, C. Chekuri, M. Pál, and J. Vondrák, "Maximizing a submodular set function subject to a matroid constraint," in *International Conference on Integer Programming and Combinatorial Optimization*. Springer, 2007, pp. 182–196.
- [12] M. Feldman, J. Naor, and R. Schwartz, "A unified continuous greedy algorithm for submodular maximization," in *2011 IEEE 52nd Annual Symposium on Foundations of Computer Science*. IEEE, 2011, pp. 570–579.
- [13] A. Anis, A. Gadde, and A. Ortega, "Efficient sampling set selection for bandlimited graph signals using graph spectral proxies," *IEEE Transactions on Signal Processing*, vol. 64, no. 14, pp. 3775–3789, 2016.
- [14] S. Chen, R. Varma, A. Sandryhaila, and J. Kovavcević, "Discrete signal processing on graphs: Sampling theory? pub_newline=""?," *IEEE transactions on signal processing*, vol. 63, no. 24, pp. 6510–6523, 2015.
- [15] S. Chen, R. Varma, A. Singh, and J. Kovavcević, "Signal recovery on graphs: Fundamental limits of sampling strategies," *IEEE Transactions on Signal and Information Processing over Networks*, vol. 2, no. 4, pp. 539–554, 2016.
- [16] A. Hashemi, R. Shafipour, H. Vikalo, and G. Mateos, "Accelerated sampling of bandlimited graph signals," *arXiv preprint arXiv:1807.07222*, 2018.
- [17] A. Jayawant and A. Ortega, "A distance-based formulation for sampling signals on graphs," in *2018 IEEE International Conference on Acoustics, Speech and Signal Processing (ICASSP)*. IEEE, 2018, pp. 6318–6322.
- [18] P. D. Sampson, A. A. Szpiro, L. Sheppard, J. Lindström, and J. D. Kaufman, "Pragmatic estimation of a spatio-temporal air quality model with irregular monitoring data," *Atmospheric Environment*, vol. 45, no. 36, pp. 6593–6606, 2011.
- [19] W. Min and L. Wynter, "Real-time road traffic prediction with spatio-temporal correlations," *Transportation Research Part C: Emerging Technologies*, vol. 19, no. 4, pp. 606–616, 2011.
- [20] S. D. Babacan, M. Luessi, R. Molina, and A. K. Katsaggelos, "Sparse bayesian methods for low-rank matrix estimation," *IEEE Transactions on Signal Processing*, vol. 60, no. 8, pp. 3964–3977, 2012.
- [21] J. Luttinen, "Fast variational Bayesian linear state-space model," in *Joint European Conference on Machine Learning and Knowledge Discovery in Databases*. Springer, 2013, pp. 305–320.
- [22] H.-F. Yu, N. Rao, and I. S. Dhillon, "Temporal regularized matrix factorization for high-dimensional time series prediction," in *Advances in neural information processing systems*, 2016, pp. 847–855.
- [23] T. Zhou, H. Shan, A. Banerjee, and G. Sapiro, "Kernelized probabilistic matrix factorization: Exploiting graphs and side information," in *Proceedings of the 2012 SIAM international Conference on Data mining*. SIAM, 2012, pp. 403–414.
- [24] I. Barjasteh, R. Forsati, D. Ross, A.-H. Esfahanian, and H. Radha, "Cold-start recommendation with provable guarantees: A decoupled approach," *IEEE Transactions on Knowledge and Data Engineering*, vol. 28, no. 6, pp. 1462–1474, 2016.
- [25] D. S. Hochbaum, "Approximating covering and packing problems: set cover, vertex cover, independent set, and related problems," in *Approximation algorithms for NP-hard problems*, 1996, pp. 94–143.
- [26] CPCB, "Delhi real time air quality data," 2019. [Online]. Available: <https://cpcb.nic.in/real-time-air-quality-data>
- [27] Y. Liu, W. Guo, K. You, L. Zhao, T. Peng, and W. Wang, "Graph learning for spatiotemporal signals with long-and short-term characterization," *IEEE Transactions on Signal and Information Processing over Networks*, vol. 6, pp. 699–713, 2020.
- [28] OTD-Delhi, "Open transit data - delhi," 2020. [Online]. Available: <https://opendata.iiitd.edu.in>

7 APPENDIX

7.1 Proof of Theorem 1

Let θ_t be the set of locations that corresponds sampled locations in the sampling matrix Θ for time stamp (column) t . The FLS gain is defined as:

$$FLS(\mathcal{M}) = \frac{\sum_{t \in \mathcal{T}} \sum_{l \in \mathcal{L}} \pi_t^l(\mathcal{M})}{L \times T} \quad (20)$$

where

$$\pi_t^l(\mathcal{M}) = \max_{\forall m \in \theta_t(\mathcal{M})} (\mathbf{S}_{l,m}) \quad (21)$$

7.1.1 Monotone non decreasing

A function f is submodular if $\forall \mathcal{C} \subseteq \mathcal{D}$

$$f(\mathcal{C}) \leq f(\mathcal{D})$$

Proof:

Let \mathcal{C} and \mathcal{D} be the subset of buses following $\forall \mathcal{C} \subseteq \mathcal{D} \subseteq \mathcal{B}$. We define $\Theta(\mathcal{C})$ and $\Theta(\mathcal{D})$ as the sampling matrix for the subset of buses \mathcal{C} and \mathcal{D} .

Let θ_t be the set of locations that corresponds to 1 in the sampling matrix $\Theta(\mathcal{C})$ for the time stamp t and Let θ'_t be the set of locations that corresponds to 1 in the sampling matrix $\Theta(\mathcal{D})$ for the time stamp t .

$$\begin{aligned} \theta_t &= \{i\} \quad \forall \Theta_{i,t}(\mathcal{C})|_{=1} \\ \theta'_t &= \{i\} \quad \forall \Theta_{i,t}(\mathcal{D})|_{=1} \end{aligned}$$

Since $\mathcal{C} \subseteq \mathcal{D}$, therefore $\theta_t \subseteq \theta'_t \quad \forall t = 1$ to T .

For all $l \in \mathcal{L}, t \in \mathcal{T}$ we have

$$\max_{\forall m \in \theta_t} (\mathbf{S}_{l,m}) \leq \max_{\forall m \in \theta'_t} (\mathbf{S}_{l,m}) \quad (22)$$

Hence $f(\mathcal{C}) \leq f(\mathcal{D})$

7.1.2 Submodular

A function f is submodular if $\forall \mathcal{C} \subseteq \mathcal{D} \subseteq \mathcal{B}$ and $b \in \mathcal{B} \setminus \mathcal{D}$

$$f(\mathcal{C} \cup b) - f(\mathcal{C}) \geq f(\mathcal{D} \cup b) - f(\mathcal{D})$$

Consider a bus $b \in \mathcal{B} \setminus \mathcal{D}$, We add the bus b in both \mathcal{C} and \mathcal{D} and analyse the gain. Let the bus traverse the set of location G_t for a time stamp t .

$$G_t = \{i\} \quad \forall \Theta_{i,t}(b)|_{=1}$$

For all $l \in \mathcal{L}$ and $t = 1$ to T we have

$$\begin{aligned} \pi_t^l(\mathcal{C} \cup b) - \pi_t^l(\mathcal{C}) &= \max_{\forall m \in \theta_t \cup G_t} (\mathbf{S}_{l,m}) - \max_{\forall m \in \theta_t} (\mathbf{S}_{l,m}) \\ &= \max(0, \max_{\forall m \in G_t} (\mathbf{S}_{l,m}) - \max_{\forall m \in \theta_t} (\mathbf{S}_{l,m})) \end{aligned} \quad (23)$$

Since

$$\max_{\forall m \in \theta_t} (\mathbf{S}_{l,m}) \leq \max_{\forall m \in \theta'_t} (\mathbf{S}_{l,m})$$

Therefore,

$$\begin{aligned} \pi_t^l(\mathcal{C} \cup b) - \pi_t^l(\mathcal{C}) &= \max(0, \max_{\forall m \in G_t} (\mathbf{S}_{l,m}) - \max_{\forall m \in \theta_t} (\mathbf{S}_{l,m})) \\ &\geq \max(0, \max_{\forall m \in G_t} (\mathbf{S}_{l,m}) - \max_{\forall m \in \theta'_t} (\mathbf{S}_{l,m})) \end{aligned} \quad (24)$$

$$\pi_t^l(\mathcal{C} \cup b) - \pi_t^l(\mathcal{C}) \geq \max(0, \max_{\forall m \in G_t} (\mathbf{S}_{l,m}) - \max_{\forall m \in \theta'_t} (\mathbf{S}_{l,m})) \quad (25)$$

$$\pi_t^l(\mathcal{C} \cup b) - \pi_t^l(\mathcal{C}) \geq \max_{\forall m \in \theta'_t \cup G_t} (\mathbf{S}_{l,m}) - \max_{\forall m \in \theta'_t} (\mathbf{S}_{l,m}) \quad (26)$$

$$\pi_t^l(\mathcal{C} \cup b) - \pi_t^l(\mathcal{C}) \geq \pi_t^l(\mathcal{D} \cup b) - \pi_t^l(\mathcal{D}) \quad (27)$$

From Eqs (23-27) for all $l \in \mathcal{L}$ and $t = 1$ to \mathcal{T} we have,

$$f(\mathcal{C} \cup b) - f(\mathcal{C}) \geq f(\mathcal{D} \cup b) - f(\mathcal{D})$$

7.2 Prove for Corollary 1

FLST gain defined via Eq. 28 is equivalent to the RFL gain defined via Eq. 41.

$$\lambda_t^l(\mathcal{M}) = \max_{m,j \in \Theta(\mathcal{M})} (\mathbf{S}_{l,m} * \mathbf{T}_{t,j}) \quad (28)$$

$$\mathbf{T}_{t,j} = \begin{cases} \rho^{t-j}, & t \geq j \\ 0, & t < j \end{cases} \quad (29)$$

$$\pi_t^l(\mathcal{M}) = \max((\mathbf{S}_{l,m})_{\forall m \in \theta_t(\mathcal{M})}, \rho \pi_{t-1}^l(\mathcal{M})) \quad \forall l \in \mathcal{L} \quad (30)$$

Proof:

For all $l \in \mathcal{L}$ and $t = 1$ using Eq. 28 we have,

$$\lambda_1^l(\mathcal{M}) = \max(\max(\mathbf{S}_{l,m})_{\forall m \in \theta_1(\mathcal{M})}, V) \quad \forall l \in \mathcal{L} \quad (31)$$

$$V = \max(\mathbf{S}_{l,m})_{\forall m \in \theta_j(\mathcal{M})} \quad (\forall j > 1) = 0$$

Therefore,

$$\lambda_1^l(\mathcal{M}) = \max((\mathbf{S}_{l,m})_{\forall m \in \theta_1(\mathcal{M})}) \quad \forall l \in \mathcal{L} \quad (32)$$

$$\lambda_1^l(\mathcal{M}) = \pi_1^l(\mathcal{M})$$

For all $l \in \mathcal{L}$ and $t = 2$ we have,

$$\lambda_2^l(\mathcal{M}) = \max(\max(\mathbf{S}_{l,m})_{\forall m \in \theta_2(\mathcal{M})}, \max((\mathbf{S}_{l,m})_{\forall m \in \theta_1(\mathcal{M})} * \rho, 0)) \quad (33)$$

$$\lambda_2^l(\mathcal{M}) = \max(\max(\mathbf{S}_{l,m})_{\forall m \in \theta_2(\mathcal{M})}, \pi_1^l(\mathcal{M}) * \rho) \quad (34)$$

$$\lambda_2^l(\mathcal{M}) = \max((\mathbf{S}_{l,m})_{\forall m \in \theta_2(\mathcal{M})}, \rho \pi_1^l(\mathcal{M})) = \pi_2^l(\mathcal{M}) \quad (35)$$

For $l \in \mathcal{L}$ and $t = n$ suppose it is true that $\lambda_n^l(\mathcal{M}) = \pi_n^l(\mathcal{M})$ and,

$$\lambda_n^l(\mathcal{M}) = \max(\max(\mathbf{S}_{l,m})_{\forall m \in \theta_n(\mathcal{M})}, \max((\mathbf{S}_{l,m})_{\forall m \in \theta_{n-1}(\mathcal{M})} * \rho, \dots, \max((\mathbf{S}_{l,m})_{\forall m \in \theta_1(\mathcal{M})} * \rho^{n-1})) \quad (36)$$

For $l \in \mathcal{L}$ and $t = n + 1$ we have,

$$\lambda_{n+1}^l(\mathcal{M}) = \max(\max(\mathbf{S}_{l,m})_{\forall m \in \theta_{n+1}(\mathcal{M})}, \max((\mathbf{S}_{l,m})_{\forall m \in \theta_n(\mathcal{M})} * \rho, \dots, \max((\mathbf{S}_{l,m})_{\forall m \in \theta_1(\mathcal{M})} * \rho^n)) \quad (37)$$

From Eq. 36,

$$\lambda_{n+1}^l(\mathcal{M}) = \max(\max(\mathbf{S}_{l,m})_{\forall m \in \theta_{n+1}(\mathcal{M})}, \rho * \lambda_n^l(\mathcal{M})) \quad (38)$$

Hence,

$$\lambda_{n+1}^l(\mathcal{M}) = \max((\mathbf{S}_{l,m})_{\forall m \in \theta_{n+1}(\mathcal{M})}, \rho \pi_n^l(\mathcal{M})) = \pi_{n+1}^l(\mathcal{M}) \quad (39)$$

7.3 Prove of Theorem 2

Let θ_t be the set of locations that corresponds to sampled locations in the sampling matrix Θ for time stamp t . For $\pi_0 = 0$, $\rho \in [0, 1]$, the regressive facility location gain is defined by

$$RFL(\mathcal{M}) = \frac{\sum_{t \in \mathcal{T}} \sum_{l \in \mathcal{L}} \pi_t^l(\mathcal{M})}{L \times T} \quad (40)$$

where

$$\pi_t^l(\mathcal{M}) = \max((\mathbf{S}_{l,m})_{\forall m \in \theta_t(\mathcal{M})}, \rho \pi_{t-1}^l(\mathcal{M})) \quad \forall l \in \mathcal{L} \quad (41)$$

7.3.1 Monotone non decreasing

A function f is submodular if $\forall \mathcal{C} \subseteq \mathcal{D} \subseteq \mathcal{B}$

$$f(\mathcal{C}) \leq f(\mathcal{D})$$

Proof:

Let \mathcal{C} and \mathcal{D} be the subset of buses following $\forall \mathcal{C} \subseteq \mathcal{D} \subseteq \mathcal{B}$. We define $\Theta(\mathcal{C})$ and $\Theta(\mathcal{D})$ as the sampling matrix for the subset of buses \mathcal{C} and \mathcal{D} .

Let θ_t be the set of locations that corresponds to 1 in the sampling matrix $\Theta(\mathcal{C})$ for the time stamp t and Let θ'_t be the set of locations that corresponds to 1 in the sampling matrix $\Theta(\mathcal{D})$ for the time stamp t .

$$\theta_t = \{i\} \quad \forall \quad |\Theta_{i,t}(\mathcal{C})| = 1$$

$$\theta'_t = \{i\} \quad \forall \quad |\Theta_{i,t}(\mathcal{D})| = 1$$

For all $l \in \mathcal{L}$ and $t = 1$ we have

$$\max_{\forall m \in \theta_1} (\mathbf{S}_{l,m}) \leq \max_{\forall m \in \theta'_1} (\mathbf{S}_{l,m}) \quad (42)$$

For $t = 2$ we have from using Eq. (22),

$$\max((\mathbf{S}_{l,m})_{\forall m \in \theta_2}, \rho \max_{\forall m \in \theta_1} (\mathbf{S}_{l,m})) \leq \max((\mathbf{S}_{l,m})_{\forall m \in \theta'_2}, \rho \max_{\forall m \in \theta'_1} (\mathbf{S}_{l,m})) \quad (43)$$

for time stamp t we have, from using Eq. (22)

$$\begin{aligned} & \max((\mathbf{S}_{l,m})_{\forall m \in \theta_t}, \rho \max_{\forall m \in \theta_{t-1}} (\mathbf{S}_{l,m}), \dots, \rho^{t-1} \max_{\forall m \in \theta_1} (\mathbf{S}_{l,m})) \\ & \leq \max((\mathbf{S}_{l,m})_{\forall m \in \theta'_t}, \rho \max_{\forall m \in \theta'_{t-1}} (\mathbf{S}_{l,m}), \dots, \rho^{t-1} \max_{\forall m \in \theta'_1} (\mathbf{S}_{l,m})) \end{aligned} \quad (44)$$

Hence $f(\mathcal{C}) \leq f(\mathcal{D})$

7.3.2 Submodular

A function f is submodular if $\forall \mathcal{C} \subseteq \mathcal{D} \subseteq \mathcal{B}$ and $b \in \mathcal{B} \setminus \mathcal{D}$

$$f(\mathcal{C} \cup b) - f(\mathcal{C}) \geq f(\mathcal{D} \cup b) - f(\mathcal{D})$$

Consider a bus $b \in \mathcal{B} \setminus \mathcal{D}$, We add the bus b in both \mathcal{C} and \mathcal{D} and analyse the gain. Let the bus traverse the set of location G_t for a time stamp t .

$$G_t = \{i\} \quad \forall \quad |\Theta_{i,t}(b)| = 1$$

For all $l \in \mathcal{L}$ and $t = 1$ to \mathcal{T} we have

$$\begin{aligned} & \pi_t^l(\mathcal{C} \cup b) - \pi_t^l(\mathcal{C}) = \\ & \max((\mathbf{S}_{l,m})_{\forall m \in \theta_t \cup G_t}, \rho \max_{\forall m \in \theta_{t-1} \cup G_{t-1}} (\mathbf{S}_{l,m}), \dots, \rho^{t-1} \max_{\forall m \in \theta_1 \cup G_1} (\mathbf{S}_{l,m})) - \\ & \max((\mathbf{S}_{l,m})_{\forall m \in \theta_t}, \rho \max_{\forall m \in \theta_{t-1}} (\mathbf{S}_{l,m}), \dots, \rho^{t-1} \max_{\forall m \in \theta_1} (\mathbf{S}_{l,m})) \end{aligned} \quad (45)$$

Let

$$K = \max((\mathbf{S}_{l,m})_{\forall m \in \theta_t}, \rho \max_{\forall m \in \theta_{t-1}} (\mathbf{S}_{l,m}), \dots, \rho^{t-1} \max_{\forall m \in \theta_1} (\mathbf{S}_{l,m}))$$

$$\begin{aligned} & \pi_t^l(\mathcal{C} \cup b) - \pi_t^l(\mathcal{C}) = \\ & \max((\mathbf{S}_{l,m})_{\forall m \in \theta_t \cup G_t}, \rho \max_{\forall m \in \theta_{t-1} \cup G_{t-1}} (\mathbf{S}_{l,m}), \dots, \rho^{t-1} \max_{\forall m \in \theta_1 \cup G_1} (\mathbf{S}_{l,m})) - K \end{aligned} \quad (46)$$

$$\begin{aligned} & \pi_t^l(\mathcal{C} \cup b) - \pi_t^l(\mathcal{C}) = \\ & \max(0, (\mathbf{S}_{l,m})_{\forall m \in G_t} - K, \rho \max_{\forall m \in G_{t-1}} (\mathbf{S}_{l,m}) - K, \dots, \rho^{t-1} \max_{\forall m \in G_1} (\mathbf{S}_{l,m}) - K) \end{aligned} \quad (47)$$

let

$$K' = \max((\mathbf{S}_{l,m})_{\forall m \in \theta'_t}, \rho \max_{\forall m \in \theta'_{t-1}} (\mathbf{S}_{l,m}), \dots, \rho^{t-1} \max_{\forall m \in \theta'_1} (\mathbf{S}_{l,m}))$$

From Eq. 44 since $K \leq K'$ Therefore,

$$\begin{aligned} & \pi_t^l(\mathcal{C} \cup b) - \pi_t^l(\mathcal{C}) \geq \\ & \max(0, (\mathbf{S}_{l,m})_{\forall m \in G_t} - K', \rho \max_{\forall m \in G_{t-1}} (\mathbf{S}_{l,m}) - K', \dots, \rho^{t-1} \max_{\forall m \in G_1} (\mathbf{S}_{l,m}) - K') \end{aligned} \quad (48)$$

$$\begin{aligned} & \pi_t^l(\mathcal{C} \cup b) - \pi_t^l(\mathcal{C}) \geq \\ & \max((\mathbf{S}_{l,m})_{\forall m \in \theta_t \cup G_t}, \rho \max_{\forall m \in \theta_{t-1} \cup G_{t-1}} (\mathbf{S}_{l,m}), \dots, \rho^{t-1} \max_{\forall m \in \theta_1 \cup G_1} (\mathbf{S}_{l,m})) - K' \end{aligned} \quad (49)$$

$$\begin{aligned} & \pi_t^l(\mathcal{C} \cup b) - \pi_t^l(\mathcal{C}) \geq \\ & \max((\mathbf{S}_{l,m})_{\forall m \in \theta'_t \cup G_t}, \rho \max_{\forall m \in \theta'_{t-1} \cup G_{t-1}} (\mathbf{S}_{l,m}), \dots, \rho^{t-1} \max_{\forall m \in \theta'_1 \cup G_1} (\mathbf{S}_{l,m})) \\ & - \max((\mathbf{S}_{l,m})_{\forall m \in \theta'_t}, \rho \max_{\forall m \in \theta'_{t-1}} (\mathbf{S}_{l,m}), \dots, \rho^{t-1} \max_{\forall m \in \theta'_1} (\mathbf{S}_{l,m})) \end{aligned} \quad (50)$$

$$\pi_t^l(\mathcal{C} \cup b) - \pi_t^l(\mathcal{C}) \geq \pi_t^l(\mathcal{D} \cup b) - \pi_t^l(\mathcal{D}) \quad (51)$$

From Eqs (45-51) for all $l \in \mathcal{L}$ and $t = 1$ to \mathcal{T} we have,

$$f(\mathcal{C} \cup b) - f(\mathcal{C}) \geq f(\mathcal{D} \cup b) - f(\mathcal{D})$$

7.4 Creating Dense Maps from Sampled Data

We use Variational Bayesian Matrix Completion (Cold start) and Variational Bayesian Subspace Filtering (Cold start) as the extended matrix completion frameworks that handles the cold start location data imputation to evaluate the performance of the dense AQ maps. We impute the missing data using VBMC(CS) where we optimize the Eqs. (52, 54). We also impute the missing data using VBSF(CS) where we optimize the Eqs. (52, 53, 54). The matrix completion framework (VBMC) proposed in paper [20] imposes a low rank structure on the data to impute the missing data as:

$$\mathcal{L}_1 = \min_{\mathbf{A}, \mathbf{B}} \|\mathbf{P}_\Omega(\mathbf{Y} - \mathbf{A}\mathbf{B}^T)\|_F \quad (52)$$

where $\mathbf{A} \in \mathcal{R}^{L \times r}$ and $\mathbf{B} \in \mathcal{R}^{T \times r}$ and $r = \text{rank}(\mathbf{Y}) \ll \min(L, T)$ Further, VBSF [5] add a regularization on the matrix \mathbf{B} to incorporate the temporal evolution in addition to the low rankness (Eq. 52) as

$$\mathcal{R}(\mathbf{B}) = \sum_{i=1}^T \|\mathbf{b}_i - \mathbf{F}\mathbf{b}_{i-1}\| \quad (53)$$

However, these framework does not incorporate for the cold start locations. Incorporating the similarity matrix \mathbf{G} along with the low rank matrix completion framework can tackle the cold start problem [23], [24].

$$\mathcal{L}_2 = \min_{\mathbf{A}, \mathbf{C}} \|(\mathbf{G} - \mathbf{A}\mathbf{C}^T)\|_F \quad (54)$$

Refer the update equations in the papers [5], [20]. We showed the changed updated equations below:
The update for i^{th} column of \mathbf{A} for the cold start matrix completion is as follows:

$$\Xi_i^{\mathbf{A}} = \left(\hat{\gamma}_i \mathbf{I}_r + \hat{\beta} \sum_{\tau \in \Omega'_i} (\boldsymbol{\mu}_\tau^{\mathbf{B}} (\boldsymbol{\mu}_\tau^{\mathbf{B}})^T + \Xi_{\tau, \tau}^{\mathbf{B}}) + \hat{\beta}_1 (\boldsymbol{\mu}^{\mathbf{C}} (\boldsymbol{\mu}^{\mathbf{C}})^T + \Xi^{\mathbf{C}}) \right)^{-1} \quad (55)$$

$$\boldsymbol{\mu}_i^{\mathbf{A}} = \Xi_i^{\mathbf{A}} (\hat{\beta} \sum_{\tau \in \Omega'_i} \boldsymbol{\mu}_\tau^{\mathbf{B}} y_{i\tau} + \hat{\beta}_1 \boldsymbol{\mu}^{\mathbf{C}} g_i) \quad (56)$$

The update for β_1 is as follows:

$$\hat{\beta}_1 = \frac{p L^2}{\|\mathbf{G} - \mathbf{A}\mathbf{C}^T\|_F^2} \quad (57)$$

The updates Eqs. for \mathbf{C} is as follows:

$$\Gamma = \text{diag}(\gamma), \quad \Xi^{\mathbf{C}} = (\langle \beta_1 \rangle \langle \mathbf{A}^T \mathbf{A} \rangle + \Gamma)^{-1} \quad (58)$$

$$\langle \mathbf{C} \rangle = \langle \beta_1 \rangle \mathbf{G} \langle \mathbf{A} \rangle \Xi^{\mathbf{C}}, \quad (59)$$